## General Disclaimer

## One or more of the Following Statements may affect this Document

- This document has been reproduced from the best copy furnished by the organizational source. It is being released in the interest of making available as much information as possible.

- This document may contain data, which exceeds the sheet parameters. It was furnished in this condition by the organizational source and is the best copy available.

- This document may contain tone-on-tone or color graphs, charts and/or pictures, which have been reproduced in black and white.

- This document is paginated as submitted by the original source.

- Portions of this document are not fully legible due to the historical nature of some of the material. However, it is the best reproduction available from the original submission.

NASA Technical Memorandum 87138

# Interlaminar Fracture Toughness: Three-Dimensional Finite-Element Modeling for End-Notch and Mixed-Mode Flexure



P.L.N. Murthy and C.C. Chamis
*Lewis Research Center*
*Cleveland, Ohio*


Prepared for the
Symposium Toughened Composites
sponsored by American Society for Testing and Materials
Houston, Texas, March 13–15, 1985

NASA

CONTENTS



STAR Category 24

# INTERLAMINAR FRACTURE TOUGHNESS: THREE-DIMENSIONAL FINITE ELEMENT MODELING FOR END-NOTCH AND MIXED-MODE FLEXURE

P.L.N. Murthy* and C.C. Chamis†
National Aeronautics and Space Administration
Lewis Research Center
Cleveland, Ohio 44135



## ABSTRACT

A computational procedure is described for evaluating End-Notch-Flexure (ENF) and Mixed-Mode-Flexure (MMF) interlaminar fracture toughness in unidirectional fiber composites. The procedure consists of a three-dimensional finite element analysis in conjunction with the strain energy release rate concept and with composite micromechanics. The procedure is used to analyze select cases of ENF and MMF. The strain energy release rate predicted by this procedure is in good agreement with limited experimental data. The procedure is used to identify significant parameters associated with interlaminar fracture toughness. It is also used to determine the critical strain energy release rate and its attendant crack length in ENF and/or MMF. This computational procedure has considerable versatility/generality and provides extensive information about interlaminar fracture toughness in fiber composites.

## INTRODUCTION

Interlaminar delamination of composites is a type of fracture mode which needs to be carefully examined and properly considered in the design of composite structures. Regions prone to delaminations include free edges, locations of stress concentration, joints, inadvertent damaged areas and defects resulting from the fabrication procedure.

One way of properly accounting for interlaminar delamination in a design is to determine interlaminar fracture toughness parameters and then to evaluate those stress states which are likely to induce interlaminar fracture. Several test methods to determine fracture toughness have been proposed and are currently being used. These tests include: edge delamination, double-cantilever beam (constant and variable thickness), cracked-lap-shear, biaxial interlaminar fracture (ARCAN), and the recently introduced three-point bend tests for Mode II (end-notch flexure (ENF)) and mixed Modes I and II fracture (MMF). Each of these test methods has its advantages and limitations (figs. 1 and 2). These tests have been the subject of discussion and evaluation at ASTM D30.02 and D30.04 subcommittee meetings and specialty symposia sponsored by these subcommittees (refs. 1 to 3).

At this time it appears that the three-point bend tests, (ENF and MMF, fig. 2) have some unique features over the others-especially for determining

---

*Research Associate, Cleveland State University.

†Senior Research Engineer, Aerospace Structures/Composites, Structures Division.

interlaminar Mode II and mixed mode fracture toughness. These unique features stem from (1) the simplicity of the test, and (2) the ability to measure the fracture toughness parameters directly during the test. Recent research efforts at Lewis Research Center have focused on the development of a computational method (procedure) for simulating the three-point bend test and evaluating interlaminar fracture toughness in unidirectional fiber composites as determined by ENF and/or MMF. This computational procedure consists of a three-dimensional finite element analysis in conjunction with the strain energy release rate concept and with composite micromechanics. The procedure is suitable for determining global and local interlaminar fracture toughness parameters as well as critical values of these parameters. The objective of this report is to describe the computational procedure in detail and results obtained therefrom.

A unique feature of this computational procedure is the consideration of the interply layer as a distinct entity and with finite thickness. The interply layer has not previously been included in three-dimensional laminate analysis (ref. 4) and in fracture mechanics-type computations. The interply layer needs to be considered in order to compute accurately those stress fields which induce interply delamination.

## FRACTURE TOUGHNESS PREDICTIONS

MSC/NASTRAN three-dimensional finite element static analysis (FEA) with substructuring was used to determine the structural response variables (displacements, stresses, strains) required for fracture toughness predictions. These structural response variables were used subsequently with three different methods to predict the interlaminar and mixed mode fracture toughness. The three methods used are: (1) the global method, (2) the local crack closure method, and (3) the NASA Lewis "unique" local crack closure method developed during this investigation. Each method is summarized below.

### Global Method

The specific computational steps for this method are as follows (refer to fig. 2).

(1) Model the specimen with crack length (a) using three-dimensional finite elements as described later.

(2) Apply a load (P) at specimen midspan.

(3) Calculate the midspan displacement v(a) using three-dimensional FEA as described later.

(4) Induce crack extension $\Delta a$ keeping load (P) constant.

(5) Calculate the midspan deflection [$v(a + \Delta a)$].

(6) Determine the Strain Energy Release Rate (SERR), G, from

$$G = P \times [v(a + \Delta a) - v(a)]/2b\Delta a \quad (1)$$

where b is the specimen width.

(7) Repeat steps (4) to (6).

(8) Plot results for G versus a or $\Delta a$.

(9) Identify fracture toughness characteristics as described later.

(10) Examine complete stress state near crack tip.

(11) Compare with corresponding uniaxial composite strengths.

(12) Look for possible correlation of fracture toughness with composite uniaxial strengths.

The global method yields the global fracture toughness without any regard to participating and/or dominating local fracture modes.

## Local Crack Closure Method

The specific steps for this method are as follows:

(1) Perform steps (1) and (2) as in the Global Method.

(2) Calculate $(u, v, w)_a$ at the crack tip nodes.

(3) Induce crack extension $\Delta a$ keeping P constant.

(4) Calculate $(u, v, w)_{a + \Delta a}$ at the same nodes as in step (2).

(5) Apply unit forces $(f_x, f_y, f_z)$ at these nodes while keeping (P) and $(a + \Delta a)$ constant.

(6) Calculate corresponding (u, v, w) displacements.

(7) Calculate local forces required to "close" the crack in its respective planes (fig. 2) using the following equations

$$F_x = \frac{u(a + \Delta a) - u(a)}{u(f_x)} \quad (2)$$

$$F_y = \frac{v(a + \Delta a) - v(a)}{v(f_y)} \quad (3)$$

$$F_z = \frac{w(a + \Delta a) - w(a)}{w(f_z)} \quad (4)$$

(8) Determine the local SERR's from

$$G_I = F_y \times [v(a + \Delta a) - v(a)]/2b\ \Delta a \quad (5)$$

$$G_{II} = F_x \times [u(a + \Delta a) - u(a)]/2b\Delta a \quad (6)$$

$$G_{III} = F_z \times [w(a + \Delta a) - w(a)]/2b\Delta a \quad (7)$$

(9) Repeat steps (3) to (8).

(10) Follow steps (8) to (12) in the Global Method.

The local crack closure method yields the contribution of each local fracture mode to the composite interlaminar or mixed mode fracture toughness. The global fracture toughness can also be determined since the midspan displacement is available from the FEA.

### NASA Lewis "Unique" Local Crack Closure Method

The specific steps for this method are as follows:

(1) Perform steps (1) to (4) in the Local Crack Closure Method.

(5) Apply enforced displacements (single point constraints) using the step (2) displacements ($u, v, w)_a$ at the crack tip nodes.

(6) Repeat FEA with these single point constraints.

(7) Calculate the corresponding forces at these constraints ($F_x$, $F_y$, $F_z$). These are called the single point constraint forces in FEA.

(8) Calculate the respective SERRs using equations (5) to (7) with the $F_x$, $F_y$, and $F_z$ from step (7).

(9) Repeat steps (1) to (8).

(10) Follow steps (8) to (12) in the Global Method.

The NASA Lewis method is a variation of the local crack closure method. The variation arises from the unique FEA feature: the single point constraint force. It is also conceptually simpler than the local crack closure method and has the added advantage of preserving the characteristic of monotonically increasing displacement under the applied load with crack extension. On the other hand, it is possible to obtain reversal in this displacement when using the local crack closure method. Comparisons of results predicted using these two methods are made in a later section.

## FINITE ELEMENT ANALYSIS MODELS

The entire specimen was modeled, including the interply layer, using the three-dimensional finite elements available in MSC/NASTRAN. A schematic of the model with the actual dimensions used is shown in figure 3. The specimen modeled is the same as that currently being evaluated by the ASTM D30.04 subcommittee for a possible standard test method to determine Mode II (using ENF) and mixed Mode I and II (using MMF) fracture toughness. The interply layers and the individual plies are modeled in the vicinity of the crack. The remaining plies are grouped as shown schematically in figure 4.

A three-dimensional computer plot of the finite element model is shown in figure 5. The specimen was modeled using 1536 solid elements for a total of 6090 degrees of freedom (DOF). A superelement was used in the crack vicinity. A two-dimensional computer plot of the superelement is shown in figure 6. The superelement contained 360 solid elements, 450 nodes (1350 DOF). The displacement boundary conditions (fig. 3) are:

$$
\begin{aligned}
&u, v = 0 \quad \text{at} \quad x, y = 0 \\
&\qquad v = 0 \quad \text{at} \quad x = \ell,\ y = 0 \qquad \text{for ENF} \\
&\qquad\qquad\qquad\quad x = \ell,\ y = \frac{t}{2} \qquad \text{for MMF} \\
&\qquad w = 0 \quad \text{at} \quad x = 0 \text{ and } \ell \\
&\qquad\qquad\qquad\quad y = 0 \qquad \text{for ENF} \\
&\qquad\qquad\qquad\quad y = \frac{t}{2} \qquad \text{for MMF} \\
&\qquad\qquad\qquad\quad z = \frac{b}{2}
\end{aligned}
\tag{8}
$$

A line load was applied at the specimen midspan (fig. 2). The magnitude of this load was 120 lb. This magnitude corresponds to the experimental load which induced unstable crack propagation as reported in the ASTM D30.02 subcommittee meeting (April 1984). The crack extension propagation was simulated by progressively deleting interply layer elements and repeating the FEA as described in the previous section. The justifications for deleting the element instead of the conventional line opening using double nodes are as follows:

(1) The interply layer element is very thin (about 10 percent of the fiber diameter).

(2) Photomicrographs of the fractured surface generally show relatively little resin residue indicating that the interply layer is destroyed during the fracture process.

(3) The crack does not remain at the midplane of the interply layer but meanders between the fiber surfaces of the adjacent plies.

The composite material simulated was AS-graphite fiber/epoxy matrix (AS/E) unidirectional composite. The constituent material properties are summarized in table I assuming room temperature dry conditions. Five different unidirectional composites were simulated with the following fiber volume ratios (FVR): 0.30, 0.55, 0.60, 0.65, and 0.75. The unidirectional ply properties, the interply layer thickness and its properties, and the appropriate material properties required for the three-dimensional finite element analysis were generated with the aid of ICAN (Integrated Composite Analyzer), (ref. 5). The properties for the interply layers were assumed to be the same as those for the matrix. The three-dimensional composite properties (using MSC/NASTRAN designation) and interply layer thickness predicted by ICAN are summarized in table II.

Even though room temperature dry conditions were assumed in this simulation, hygrothermal environmental effects can readily be simulated using the theory (ref. 6) embedded in ICAN to predict the corresponding composite properties. Other composite systems including (1) intraply hybrids, (2) interply hybrids, (3) intra/inter ply hybrids, (4) composites with perforated interply layers, and (5) composites with different void content can readily be simulated using ICAN.

## RESULTS AND DISCUSSION

The results obtained together with appropriate discussions, interpretations, and possible implications are summarized below first for the global method and second for the local crack closure methods. The results are presented graphically where midspan displacement and SERR are plotted versus crack propagating length for the five different fiber volume ratios (FVR). In addition, graphical results are presented for the stress field behavior in the vicinity of the crack and also the variation of maximum stress magnitudes versus crack propagating length. The maximum stress magnitudes are assumed to be at the centroid of the interply element in the superelement ahead of the crack tip.

### Global Method Results

The midspan displacement versus crack propagating length for the five different fiber volume ratios is shown in figure 7 for the ENF specimen. The midspan displacement decreases with increasing fiber volume ratio. Also, the midspan deflection increases gradually with crack opening length up to about a $\simeq$1.20 in, and then increases rapidly. The corresponding SERR $G_{II}$ determined using the global method described previously (Eq. (1)) is shown in figure 8. The authors interpret the behavior shown in figure 8 to be associated with interlaminar composite fracture characteristics as follows:

(1) The initial portion of the curves ($a < 1.05$ in) represents slow crack growth.

(2) The intermediate portion ($1.05$ in $< a < 1.20$ in) represents stable crack growth.

(3) The rapid increase (rise) ($a \geq 1.20$ in) represents unstable, and therefore rapid crack propagation to fracture.

The SERR $G_{II}$ varies approximately inversely with FVR as would be expected since it is calculated from the midspan displacement which also varies inversely with FVR.

The corresponding results for MMF are shown in figure 9 for displacement and in figure 10 for SERR G. These curves exhibit the same behavior as those for ENF and, therefore, exhibit similar interlaminar composite fracture characteristics. A comparison of the curves in figures 8 and 10 reveals that the interlaminar fracture characteristics for ENF and MMF are almost identical for the same load. Again, this is anticipated since they are both determined using the midspan displacement which is about the same for the two cases.

The results in figures 8 and 10 show that the anticipated "global" composite interlaminar fracture strain energy release rate can be predicted by conducting three-dimensional finite element analyses on ENF and MMF specimens and using the global method. In addition, these results show similar characteristics for shear (Mode II) and mixed (Mode I and II) fracture. One conclusion from the above discussion is that the global method is quite general for determining the mixed mode composite interlaminar fracture characteristics. Embedded cracks, multiple cracks, crack location, specimens of uniform and variable cross sections, and different laminate configurations can be just as easily handled as the two cases already described. The global method generally does not separate the contribution of each mode. However, these contributions can be determined by the local crack closure methods as described in the next section.

## Local Crack Closure Methods Results

The Mode II SERR, determined using the local crack closure method (eq. (6)), is shown in figure 11 (dashed line) for 0.6 FVR. The curve determined using the global method is also plotted for comparison. The range of experimental data reported in the ASTM D30.02 subcommittee meeting is shown by dashed horizontal lines. Three points are worth noting in figure 11:

(1) The global method predicts higher $G_{II}$ values than the local crack closure method.

(2) The two methods predict similar composite intralaminar fracture behavior.

(3) The measured data coincide with the rapid rise in both curves.

Accordingly, two general conclusions can be drawn:

(1) The rapid rise in the SERR ($G_{II}$) versus crack length (a) coincides with the measured critical $G_{II}$.

(2) A conservative assessment of the composite interlaminar fracture characteristics can be obtained by using the $G_{II}$ determined from the local crack closure method.

The mixed mode (I and II) composite interlaminar fracture characteristics, determined from the local crack closure method (eqs. (5) and (6)), are shown in figure 12 for a composite with 0.6 FVR. The fracture characteristics for each mode (Mode I and Mode II) are compared with those predicted for the mixed mode by using the global method (solid line) and the algebraic sum of the two modes from the local method (short dashed line). The following observations are worth noting in figure 12:

(1) Both the local crack closure and the global methods predict similar mixed mode (Mode I and II) fracture characteristics.

(2) The local crack closure method predicts lower mixed mode G values than the global method.

(3) Mode II fracture dominates the crack extension during slow and stable crack growth ($a < 1.05$ in).

(4) Mode I dominates the crack extension during unstable crack growth and rapid crack propagation ($a > 1.15$ in).

(5) Mode I has slightly negative values ($a < 1.15$ in) indicating local v (predicted by eq. 5) displacement reversal.

The general conclusions to be drawn from the above observations are:

(1) The contribution of each fracture mode can be determined using the local crack closure method.

(2) Mode I drives the composite interlaminar delamination in MMF specimens.

(3) The local method provides a conservative assessment of mixed mode composite interlaminar fracture characteristics as was the case for Mode II.

The mixed mode (Mode I and II) composite interlaminar fracture characteristics predicted using the Lewis method (local single point constraints) are shown in figure 13. The characteristics predicted by using this method are practically the same as those observed in figure 12. One exception is that Mode I is positive for all 'a' and, thus, this method preserves the v displacement monotonicity. A typical value for $G_I$ is about 0.6 psi-in at the onset of rapid crack propagation for this type of composite. This coincides with the rapid rise in Mode I (figs. 12 and 13). It is important to note that the contribution of each mode to mixed mode fracture can be determined, within acceptable engineering accuracy, by either of the local methods described herein. The local crack closure method, however, is easier to implement computationally based on the authors' research experience.

The composite interlaminar opening mode fracture was also determined by simulating a double cantilever beam (DCB) specimen with the same geometry and loads used in the ENF and MMF. The results are shown in figure 14 for both the global and the local methods. The general fracture characteristics are similar to those determined for Mode I by the local methods of the MMF (figs. 12 and 13). The significant exception is that the opening fracture mode of the DC specimen becomes unstable at a smaller crack opening compared to the MMF specimen.

Apparently the presence of Mode II increases the resistance to Mode I fracture. This is consistent with experimental observations (ref. 7). The significant conclusion is that the local crack closure methods predict the magnitude of the opening mode contribution and its dominance to rapid crack propagation in mixed mode fracture reasonably well.

## LOCAL STRESS FIELDS

End-Notch-Flexure. - The averaged across-the-width stress field behavior in the interply layer in the ENF is shown in figure 15. Interestingly, all three stresses $\sigma_{xx}$, $\sigma_{yy}$, and $\sigma_{xy}$ have approximately the same magnitude in the element next to the crack tip. The two normal stresses ($\sigma_{xx}$ and $\sigma_{yy}$)

are compressive, monotonic, and decay rapidly with distance from the crack tip as would be expected from the near-singular stress field. On the other hand, the shear stress exhibits oscillatory behavior near the crack tip, decreases to a relatively constant value and then slowly decays to the value predicted by simple beam theory. At this time the authors suspect that this oscillatory behavior may be real. Two supporting reasons are:

(1) The proper behavior of the two normal stresses gives confidence in the analysis, and

(2) The relatively constant value of the shear stress at a distance from the crack-tip greater than 0.05 in.

The peak stress field behavior (stress in the interply layer crack tip element) versus the extending crack length is shown in figure 16 for 0.6 FVR. Also shown in this figure is the interlaminar shear strength predicted by using the composite micromechanics equations programmed in ICAN. The peak shear stress ($\sigma_{xy}$) reaches relatively high values during the slow crack growth stage and remains practically constant during the stable crack growth stage (fig. 8). The peak shear stress exceeds the corresponding strength for practically the entire extending crack distance. The peak value of the through-the-thickness normal stress ($\sigma_{yy}$) is substantial (comparable to $\sigma_{xx}$) and it is compressive throughout the extending crack distance. This compressive normal stress will tend to close the crack and thus enhance the interlaminar resistance to Mode II type fracture.

It appears that the rise in the peak shear stress is associated with an increase in the normal compressive $\sigma_{yy}$ stress. The peak normal stress ($\sigma_{xx}$), along the specimen span, is also compressive and has about the same magnitude as $\sigma_{yy}$. Both of the normal compressive stresses tend to crush the fractured interply layer and, therefore, provide additional credence to simulating the extending crack by deleting the interply layer crack-tip element.

The significant conclusion from the above discussion is that interply Mode II fracture occurs when the corresponding shear strength is exceeded. This conclusion can be used to determine critical fracture toughness parameters as will be described later.

Mixed-Mode-Flexure. - The corresponding average stress-field behavior in the MMF is shown in figure 17. The two normal stresses ($\sigma_{yy}$ and $\sigma_{xx}$) exhibit singular monotonic stress behavior while the shear stress ($\sigma_{xy}$) exhibits oscillatory behavior near the crack tip and becomes constant thereafter. Three points worth noting are:

(1) $\sigma_{yy}$ has the highest magnitude in the crack-tip element.

(2) Both normal stresses are tensile while they were compressive in the ENF specimen.

(3) The shear stress magnitude beyond the crack tip vicinity is about the same as that in the ENF flexure specimen (fig. 15).

The peak stresses in the MMF specimen versus extending crack-tip distance are shown in figure 18. Also shown in this figure are the corresponding interlaminar shear and transverse tensile strengths predicted using ICAN.

Both stresses ($\sigma_{yy}$ and $\sigma_{xy}$) exceed their corresponding strengths for practically the entire extending crack-tip distance. Additionally, $\sigma_{yy}$ rises more rapidly while $\sigma_{xy}$ remains approximately constant for extending crack-tip distances greater than 0.150 in. These result are consistent with the SERR G behavior (fig. 10) and demonstrate that the MMF specimen is subjected to both opening mode (Mode I) and shear mode (Mode II) type fractures.

The significant conclusion from the above discussion is that mixed mode fracture occurs in MMF specimens when the stresses $\sigma_{yy}$ and/or $\sigma_{xy}$ exceed their corresponding strengths. This is consistent with the conclusion stated previously for the ENF specimen. It has the same significant implications and can be used to determine mixed mode fracture toughness as will be described later.

## FRACTURE TOUGHNESS PARAMETERS

During the course of this investigation, it became evident that composite interlaminar fracture toughness is associated with several intrinsic properties of the composite. The most obvious ones include interply layer thickness, interlaminar shear strength and transverse tensile strength. These are in addition to the well known critical strain energy release rate (SERR), critical stress intensity factor and crack length. Furthermore, the intrinsic composite properties depend on composite constituent material properties and on fiber volume ratio (FVR) and, as a result, are not independent. Their interdependence can be determined by composite micromechanics (refs. 8 and 9).

The effects of fiber volume ratio on the fracture toughness parameters are presented graphically in figure 19 for ENF (Mode II) fracture and for a 120 lb load. The parameters plotted are: interlaminar shear strength, SERR and interply layer thickness for three different crack lengths ($\Delta a$). The interesting points to be noted are:

(1) The SERR decreases with increasing FVR (rapidly at low FVR (about 0.30) and more slowly at high FVR (about 0.70)).

(2) Both the interlaminar shear strength and the interply layer thickness decrease with increasing FVR and at a progressively faster rate.

Both of these lead to the conclusion that fiber composites with relatively high FVR will have lower fracture toughness compared to those with intermediate (about 0.5) or low FVR. Another, and perhaps by far more important, conclusion is that composite mechanics in conjunction with three-dimensional finite element analysis provide unique computational analysis methods for describing/-assessing the fracture toughness of fiber composites in general.

## PREDICTION OF COMPOSITE INTERLAMINAR FRACTURE TOUGHNESS

The results of this investigation taken collectively lead to a general computational procedure for predicting unidirectional composite interlaminar fracture toughness using the End-Notch-Flexure (ENF) and/or Mixed-Mode-Flexure (MMF) methods. In developing this procedure, the critical parameters associated with the fracture toughness of the composite are revealed. This procedure consists of the following steps:

(1) Determine the requisite properties at the desired conditions using composite micromechanics. These requisite properties will be similar to those summarized in table II.

(2) Run a three-dimensional finite element analysis on an ENF or MMF specimen (fig. 2) for an arbitrary load using finite element models similar to those described herein (figs. 3 and 4). Note that the superelement is not necessary although it expedites the computations.

(3) Scale the arbitrary load in step (2) to match interlaminar shear stress or through-the-thickness normal stress in the crack-tip element with the interlaminar shear strength or the through-the-thickness normal strength of the composite. Note that this element is next to the crack tip.

(4) Run several finite element analyses with the scaled load and progressively extending crack length (a).

(5) Calculate strain energy release rates (G) using the appropriate equations (eqs. (1), (5), (6), or (7)).

(6) Plot the curve G calculated at step (5) versus a. This curve is similar to those in figures 11 to 13.

(7) Construct two tangents to the curve as follows:
   (a) through the slowly rising portion of the stable crack growth region
   (b) through the rapidly rising portion of the unstable crack growth region.

(8) Select the critical G (strain energy release rate) value and the critical crack-length from the intersection of the two tangents in step (7). The steps for this procedure are summarized together with a schematic in figure 20 for convenience.

It is important to note that this procedure has not been verified with appropriate experimental data other than that described herein. Therefore, it should be used judiciously until sufficently well validated. However, it provides a convenient computational method for initial screening of candidate composites to select those which should meet interlaminar fracture toughness design requirements. It also provides a direct means for quantifying values for critical strain energy release rate (G) and its corresponding critical length (a) on which design criteria can be based. It is the authors' considered technical judgment that proper use of this computational procedure provides detailed information which can be used to describe, assess, and predict composite interlaminar fracture toughness. As a result, composite structures can be designed to meet this hitherto elusive critical design requirement. This computational procedure has considerable versatility and generality as was previously discussed.

## SUMMARY OF RESULTS

The significant results of an investigation of composite interlaminar fracture determined by the computational simulation of end-notch-flexure (ENF) and mixed-mode-flexure (MMF) are summarized below:

1. Three-dimensional finite element analysis in conjunction with composite mechanics provides a direct computational method for determining the interlaminar fracture toughness in unidirectional composites.

2. The significant composite properties associated with composite interlaminar fracture toughness are: (a) interlaminar shear strength, (b) transverse tensile strength, (c) interply layer thickness, and (d) fiber volume ratio.

3. Three methods are suitable to computationally determine the interlaminar strain energy release rate (SERR): (a) the global method, (b) the local crack closure method, (c) the local single point constrained force (Lewis) method. However, only the local methods are suitable for determining the contributions of each fracture mode.

4. The global method predicts higher SERR compared to local methods during slow and stable crack growth. However, all three methods tend to converge during rapidly increasing strain energy release rate (SERR) which indicates unstable crack growth.

5. Predicted SERR for shear (Mode II) and mixed mode (I and II) interlaminar fracture are in good agreement with limited measured data.

6. Mode II (shear) dominates ENF while Mode I (opening) dominates the unstable crack growth in MMF.

7. Mode II (shear) unstable crack growth occurs in ENF when the interlaminar shear stress intensity (as determined herein) exceeds its corresponding shear strength.

8. Mixed mode (I and II) unstable crack growth occurs in MMF when the through-the-thickness normal stress intensity (as determined herein) exceeds its corresponding transverse tensile strength.

9. A computational procedure was developed to determine the critical SERR and its attendant crack length associated with ENF and/or MMF fracture.

## REFERENCES


1. Sendeckyj, G.P., Ed., Fracture Mechanics of Composites, ASTM STP-593, American Society for Testing and Materials, Philadelphia, PA, 1975.

2. Reifsnider, K.L., Ed., Damage in Composite Materials, ASTM STP-775, American Society for Testing and Materials, Philadelphia, PA, 1982.

3. Wilkins, D.J., Ed., Effects of Defects in Composite Materials, ASTM STP-836, American Society for Testing and Materials, Philadelphia, PA, 1984.

4. Murthy, P.L.N. and Chamis C.C., Computers and Structures, Vol. 20, No. 1-3, 1985, pp. 431-441.

5. Murthy, P.L.N. and Chamis, C.C., "ICAN: Integrated Composites Analyzer," AIAA Paper 84-0974, American Institute of Aeronautics and Astronautics, New York, May 1984.

6. Chamis, C.C., Lark, R.F., and Sinclair, J.H., in Advanced Composite Materials - Environmental Effects, ASTM STP-658, J.R. Vinson, Ed., American Society for Testing and Materials, Philadelphia, 1978, pp. 160-192.

7. Vanderkley, P.S., "Mode I - Mode II Delamination Fracture Toughness of a Unidirectional Graphite/Epoxy Composite," Master of Science Thesis, Texas A & M University, 1981.

8. Chamis, C.C., SAMPE Quarterly, Vol. 15, No. 3, Apr. 1984, pp. 14-23.

9. Chamis, C.C., SAMPE Quarterly, Vol. 15, No. 4, July 1984, pp. 41-55.

TABLE I. - CONSTITUENT MATERIAL PROPERTIES USED IN THE SIMULATION

| Property | Units | Fiber AS-graphite | | Matrix intermediate-modulus high-strength | |
|---|---|---|---|---|---|
| | | Symbol | Value | Symbol | Value |
| Elastic moduli | $x10^6$ psi | $E_{f11}$ | 31.00 | $E_m$ | 0.5 |
| | | $E_{f22}$ | 2.00 | | |
| | | $G_{f12}$ | 2. | | |
| | | $G_{f23}$ | 1. | $G_m$ | .1852 |
| Poisson's ratio | -------- | $\nu_{f12}$ | 0.2 | $\nu_m$ | .35 |
| | | $\nu_{f23}$ | 0.25 | | |
| Strengths | ksi | $S_{fT}$ | 400 | $S_{mT}$ | 15 |
| | | $S_{fc}$ | 400 | $S_{mc}$ | 35 |
| | | | | $S_{ms}$ | 13 |
| Fiber diameter | inch | $d_f$ | 0.0003 | | |

TABLE II. - COMPOSITE PROPERTIES PREDICTED BY ICAN AND USED IN THREE-DIMENSIONAL FINITE ELEMENTS

| Property | Units | MSC/NASTRAN Designation | | | | | |
|---|---|---|---|---|---|---|---|
| | | Symbol | Fiber volume ratio | | | | |
| | | | 0.30 | 0.55 | 0.60 | 0.65 | 0.75 |
| Elastic constants in the stress/strain relationship for unidirectional AS/E composite | $\times 10^6$ lb/in$^2$ | G11 | 12.420 | 20.023 | 21.478 | 22.921 | 25.782 |
| | | G21 = G12 | 0.734 | 0.629 | 0.615 | 0.602 | 0.583 |
| | | G31 = G13 | .734 | .629 | .615 | .602 | .583 |
| | | G41 = G14 | .000 | .000 | .000 | .000 | .000 |
| | | G51 = G15 | .000 | .000 | .000 | .000 | .000 |
| | | G61 = G16 | .000 | .000 | .000 | .000 | .000 |
| | | G22 | 1.412 | 1.511 | 1.549 | 1.593 | 1.704 |
| | | G32 = G23 | .863 | .731 | .710 | .691 | .654 |
| | | G42 = G24 | .000 | .000 | .000 | .000 | .000 |
| | | G52 = G25 | .000 | .000 | .000 | .000 | .000 |
| | | G62 = G26 | .000 | .000 | .000 | .000 | .000 |
| | | G33 | 1.544 | 1.620 | 1.654 | 1.694 | 1.800 |
| | | G43 = G34 | .000 | .000 | .000 | .000 | .000 |
| | | G53 = G35 | .000 | .000 | .000 | .000 | .000 |
| | | G63 = G36 | .000 | .000 | .000 | .000 | .000 |
| | | G44 | .368 | .566 | .623 | .690 | .865 |
| | | G54 = G45 | .000 | .000 | .000 | .000 | .000 |
| | | G64 = G46 | .000 | .000 | .000 | .000 | .000 |
| | | G55 | .245 | .336 | .362 | .394 | .476 |
| | | G65 = G56 | .000 | .000 | .000 | .000 | .000 |
| | | G66 | .368 | .566 | .623 | .690 | .865 |
| Interply layer properties | | | | | | | |
| moduli | $\times 10^6$ lb/in$^2$ | E | .5 | .5 | .5 | .5 | .5 |
| | --- | v | .35 | .35 | .35 | .3 | .35 |
| Thickness | incn | δ | $0.1854\times10^{-3}$ | $0.5850\times10^{-4}$ | $0.4323\times10^{-4}$ | $0.2977\times10^{-4}$ | $0.6998\times10^{-5}$ |

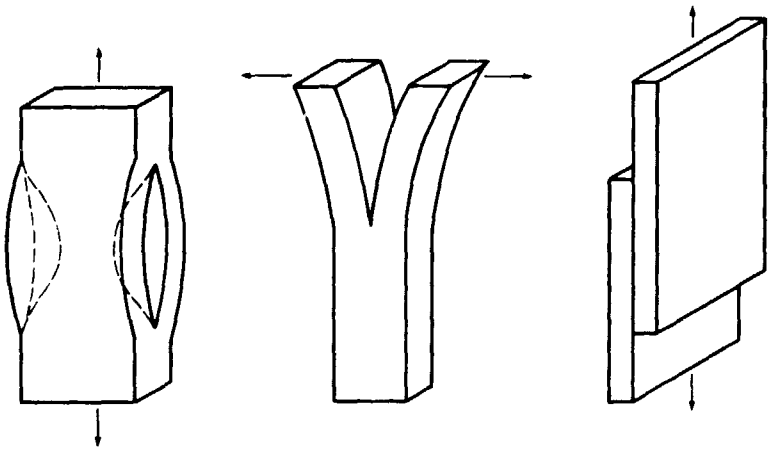


Figure 1. - Schematics of test methods for measuring interlaminar fracture toughness.

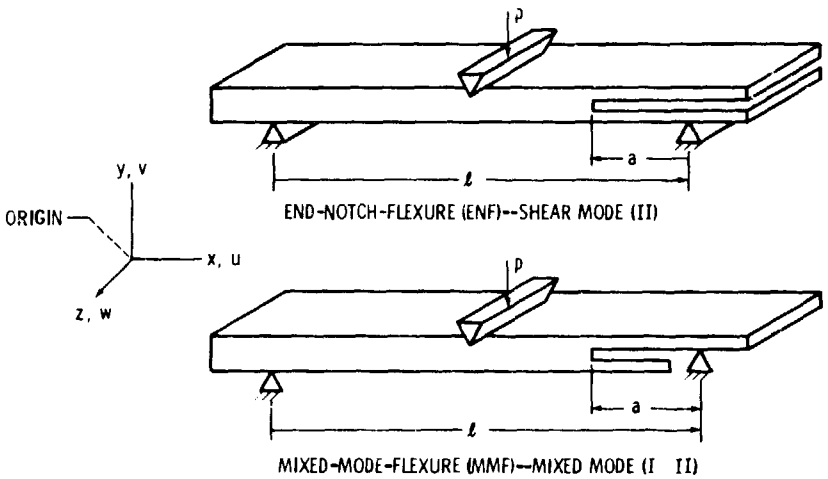


Figure 2. - Schematic of flexural test for interlaminar fracture mode toughness.
Note: Origin at left support bottom.

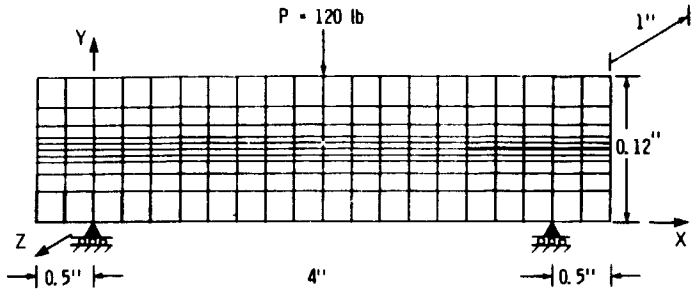


Figure 3. - Model geometry and F.E. schematic.

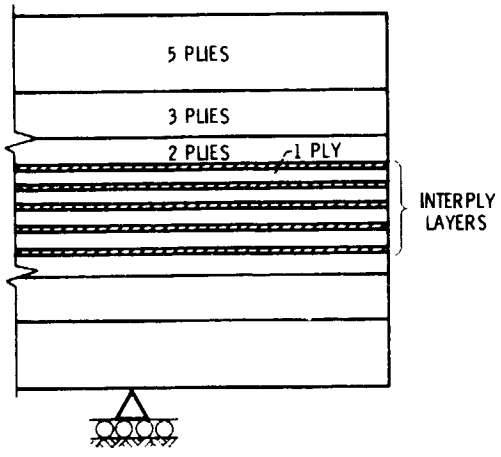


Figure 4. - Schematic of F.E. model through-the-thickness details.

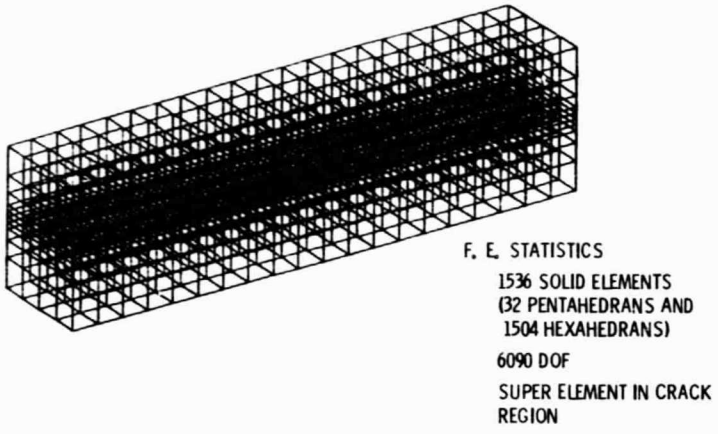


Figure 5. - 3-D finite element model.

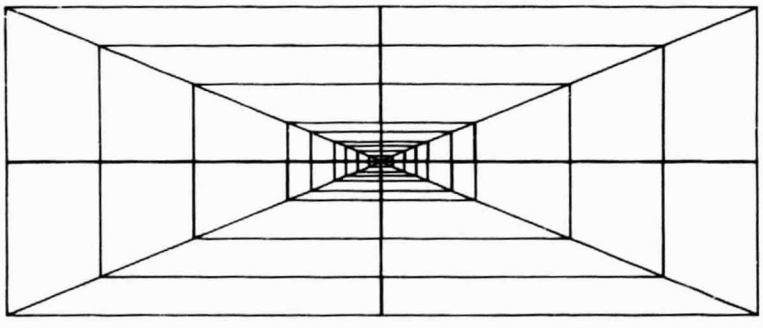

Figure 6. - Crack region superelement model details-front view. Superelement statistics: 360 solid elements (32 6-node pentahedrans, 328 8-node bricks) 450 nodes, 1350 DOF.

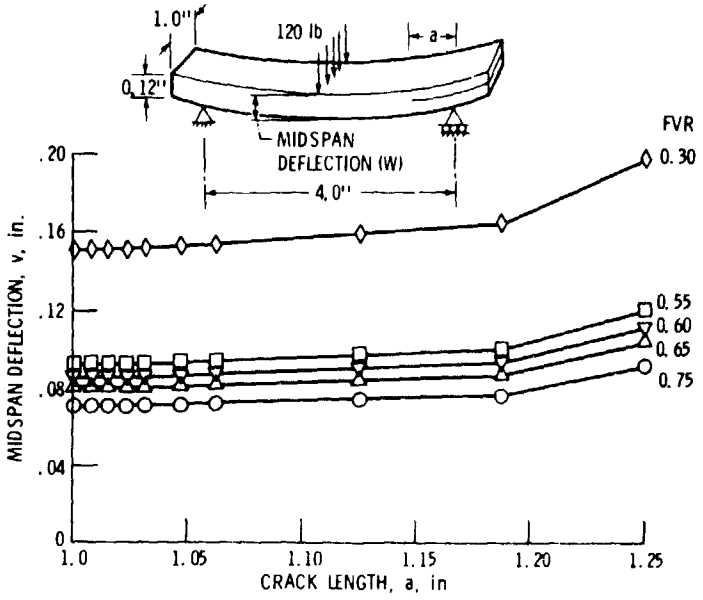


Figure 7. - Fiber volume ratio effects on midspan deflection. End-notch-flexure (AS/E).

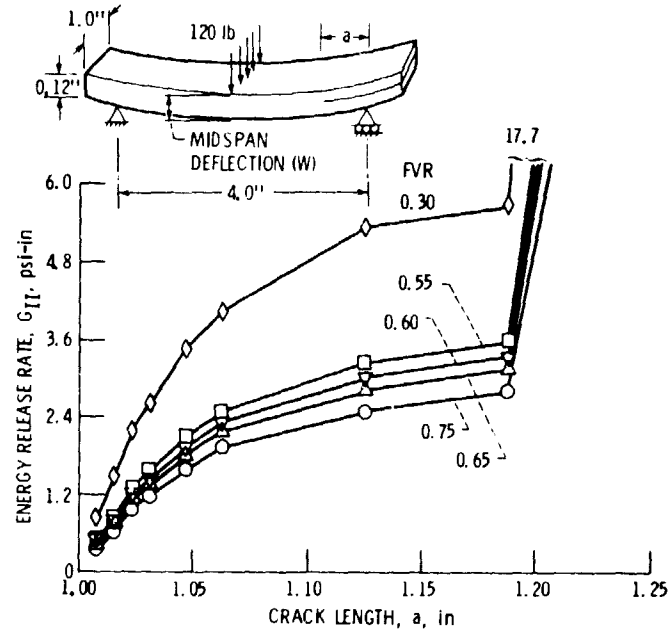


Figure 8. - Fiber volume ratio effects on Mode II energy release rate. End-notch-flexure (AS/E).

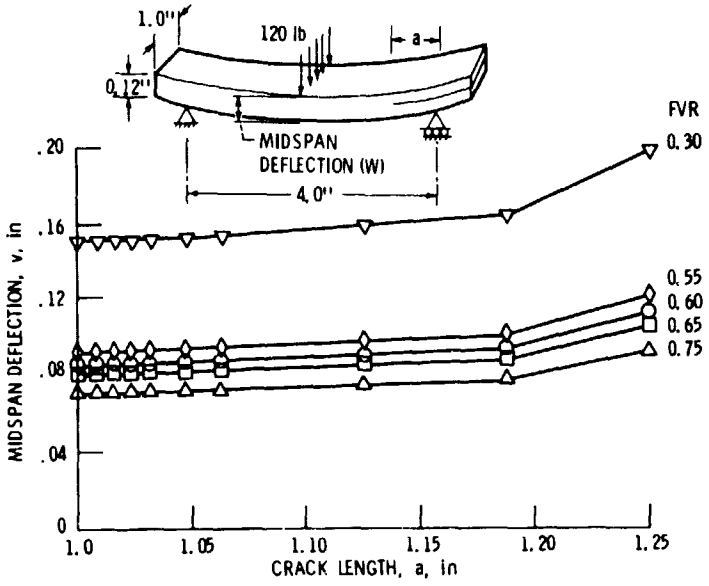


Figure 9. - Fiber volume ratio effects on midspan deflection. Mixed-mode-flexure (AS/E).

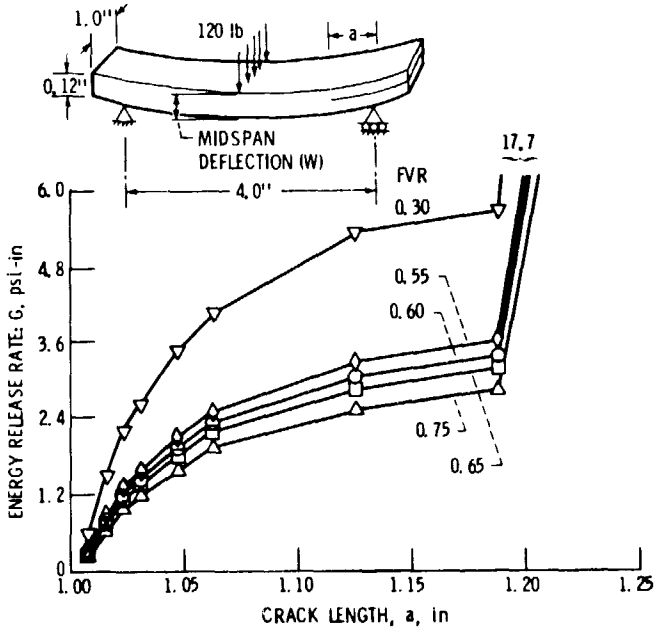


Figure 10. - Fiber volume ratio effects on mixed mode (I & II). Mixed-mode-flexure (AS/E).

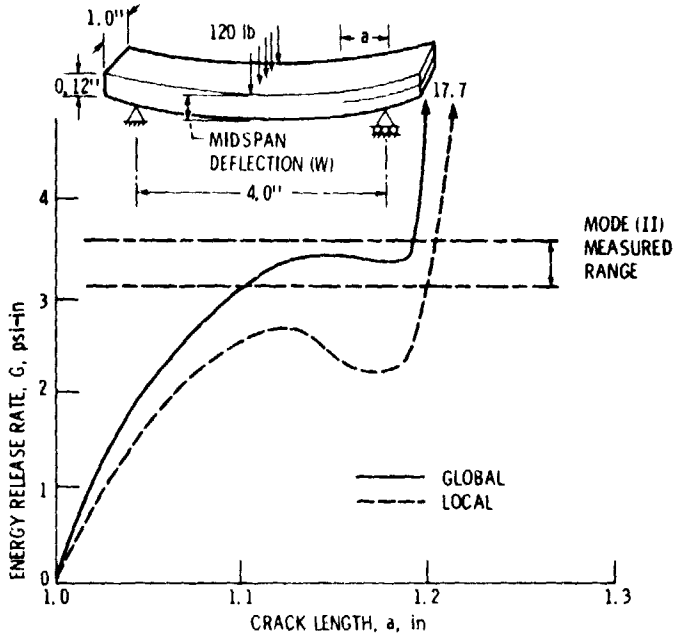


Figure 11. - End-notch flexure energy release rate-comparison.

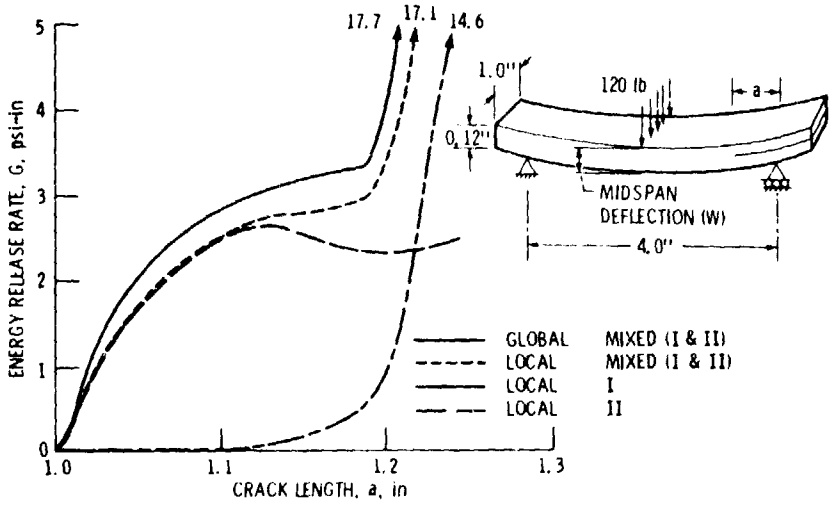


Figure 12. - Mixed-mode-flexure energy release rate and components (AS/E). Local closure method.

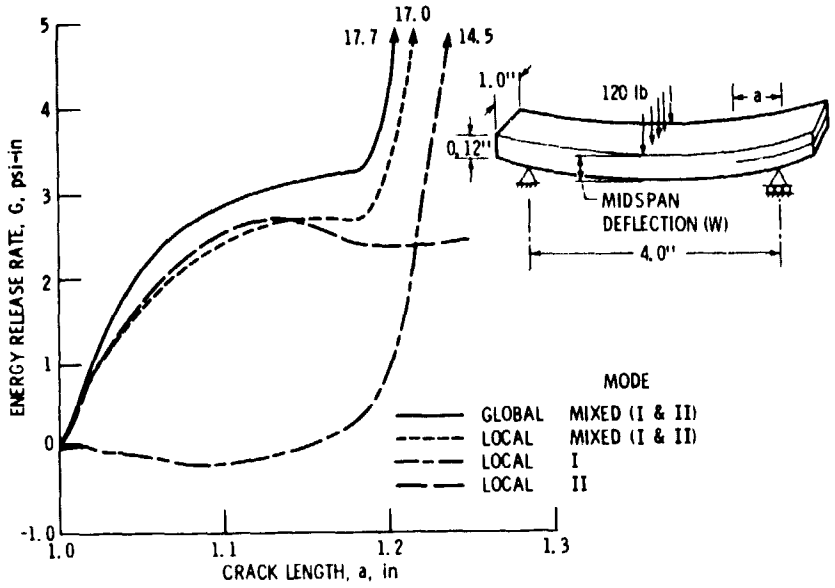


Figure 13. - Mixed-mode flexure energy release rate and components (AS/E). Single point constrained (Lewis) method.

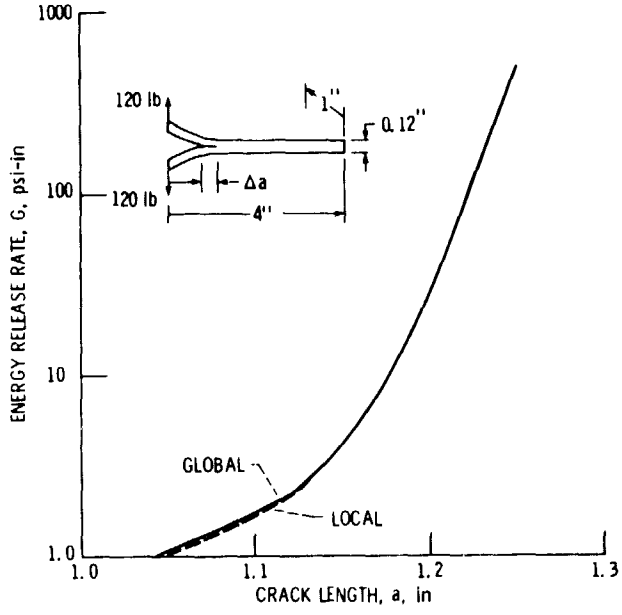


Figure 14. - Double-cantilever energy release rate-comparisons (AS/E).

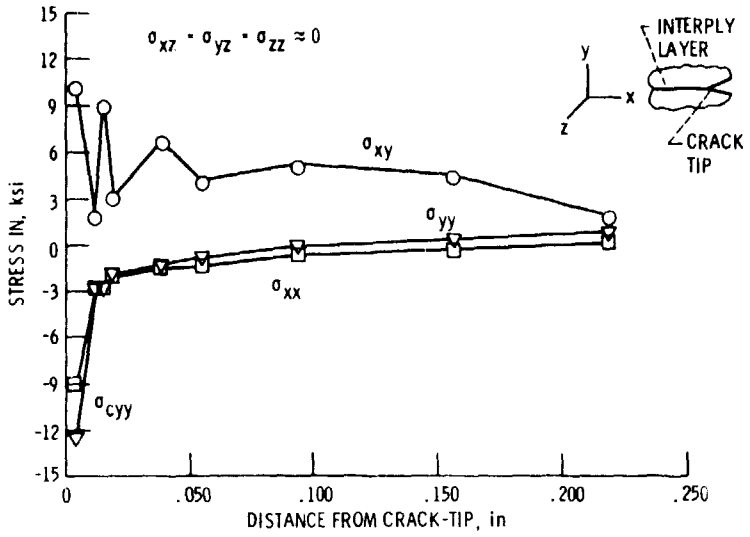


Figure 15. - Stress field in interply layer near crack tip. End-notch-flexure (AS/E).

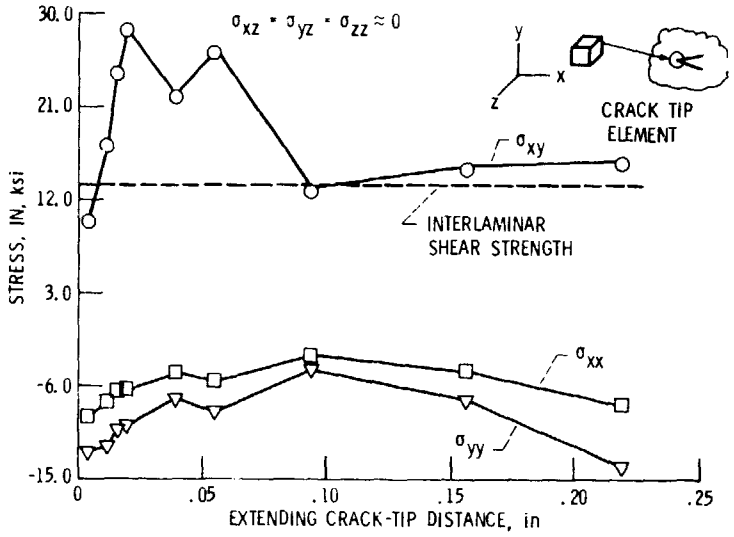


Figure 16. - Peak stress behavior in interply layer with crack extension. End-notch-flexure (AS/E).

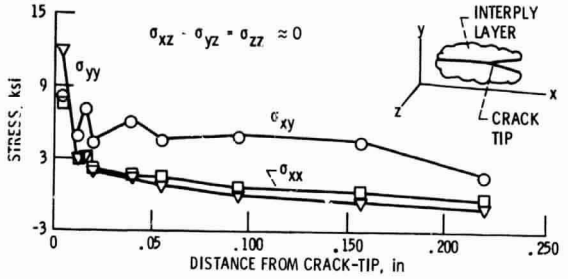


Figure 17. - Stress field in interply layer near crack tip. Mixed-mode-flexure (AS/E).

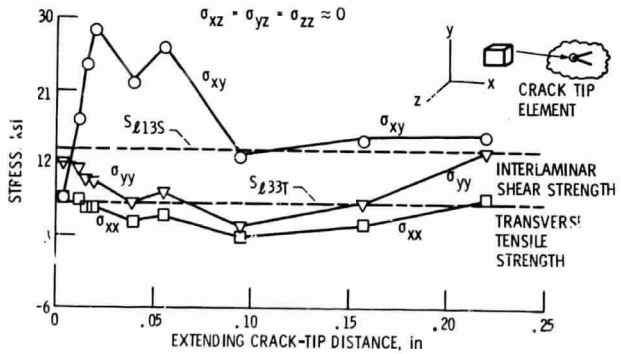


Figure 18. - Peak stress behavior at crack tip with crack extension. Mixed-mode-fracture (AS/E).

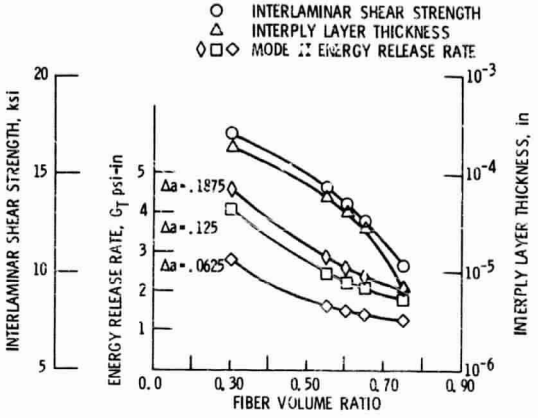


Figure 19. - Fiber volume ratio effect on interlaminar fracture toughness parameters, End-notch-flexture (AS/E).

- DETERMINE REQUISITE PROPERITES AT DESIRED CONDITIONS USING COMPOSITE MICROMECHANICS
- RUN 3-D FINITE ELEMENT ANALYSIS ON ENF (MMF) SPECIMEN FOR AN ARBITRARY LOAD
- SCALE LOAD TO MATCH INTERLAMINAR SHEAR STRESS AT ELEMENT NEXT TO CRACK-TIP
- WITH SCALED LOAD EXTEND CRACK AND PLOT STRAIN ENERGY RELEASE RATE VS CRACK LENGTH
- SELECT CRITICAL "G" AND CRITICAL "a"
- METHOD HAS VERSATILITY/GENERALITY

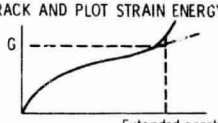


Figure 20. - General procedure for predicting composite interlaminar fracture toughness using the end-notch-flexure (ENF) or mixed-mode-flexure (MMF) method.

| 1. Report No. | 2. Government Accession No. | 3. Recipient's Catalog No. |
|---|---|---|
| NASA TM-87138 | | |

| 4. Title and Subtitle | 5. Report Date |
|---|---|
| Interlaminar Fracture Toughness: Three-Dimensional Finite Element Modeling For End-Notch and Mixed-Mode Flexure | 6. Performing Organization Code: 505-33-7B |
| 7. Author(s): P.L.N. Murthy and C.C. Chamis | 8. Performing Organization Report No.: E-2626 |
| | 10. Work Unit No. |
| 9. Performing Organization Name and Address: National Aeronautics and Space Administration, Lewis Research Center, Cleveland, Ohio 44135 | 11. Contract or Grant No. |
| 12. Sponsoring Agency Name and Address: National Aeronautics and Space Administration, Washington, D.C. 20546 | 13. Type of Report and Period Covered: Technical Memorandum |
| | 14. Sponsoring Agency Code |

15. Supplementary Notes

Prepared for the Symposium on Toughened Composites sponsored by the American Society for Testing and Materials, Houston, Texas, March 13-15, 1985.

16. Abstract

A computational procedure is described for evaluating End-Notch-Flexure (ENF) and Mixed-Mode-Flexure (MMF) interlaminar fracture toughness in unidirectional fiber composites. The procedure consists of a three-dimensional finite element analysis in conjunction with the strain energy release rate concept and with composite micromechanics. The procedure is used to analyze select cases of ENF and MMF. The strain energy release rate predicted by this procedure is in good agreement with limited experimental data. The procedure is used to identify significant parameters associated with interlaminar fracture toughness. It is also used to determine the critical strain energy release rate and its attendant crack length in ENF and/or MMF. This computational procedure has considerable versatility/generality and provides extensive information about interlaminar fracture toughness in fiber composites.

| 17. Key Words (Suggested by Author(s)) | 18. Distribution Statement |
|---|---|
| Computational procedure; Strain-energy release rate; Composite micromechanics; Shear mode; Mode II fracture; Opening mode; Mode I fracture; Global method; Local methods; Three-dimensional stresses; Composite strengths; Graphite fiber; Epoxy matrix; Crack opening; Interply layer; Fracture toughness | Unclassified - unlimited<br>STAR Category 24 |

| 19. Security Classif. (of this report) | 20. Security Classif. (of this page) | 21. No. of pages | 22. Price* |
|---|---|---|---|
| Unclassified | Unclassified | | |

*For sale by the National Technical Information Service, Springfield, Virginia 22161